Published in final edited form as:
JACC Cardiovasc Imaging. 2009 October ; 2(10): 1213–1222. doi:10.1016/j.jcmg.2009.04.016.

^{18}F-4V for PET-CT imaging of VCAM-1 expression in inflammatory atherosclerosis

Matthias Nahrendorf, MD, PhD[1,2,3], **Edmund Keliher, PhD**[1,2,*], **Peter Panizzi, PhD**[2,*], **Hanwen Zhang, PhD**[2,*], **Sheena Hembrador, BS**[2], **Jose-Luiz Figueiredo, MD**[1,2], **Elena Aikawa, MD**[2], **Kimberly Kelly, PhD**[2], **Peter Libby, MD**[3,4], and **Ralph Weissleder, MD, PhD**[1,2,3]

[1] Center for Systems Biology, Massachusetts General Hospital and Harvard Medical School, Simches Research Building, 185 Cambridge St., Boston, MA 02114

[2] Center for Molecular Imaging Research, Massachusetts General Hospital and Harvard Medical School, Building 149, 13th St., Charlestown, MA 02129

[3] Donald W. Reynolds Cardiovascular Clinical Research Center on Atherosclerosis at Harvard Medical School

[4] Cardiovascular Division, Department of Medicine, Brigham & Women's Hospital, 75 Francis Street, Boston, MA 02115

Abstract

Objectives—To iteratively develope and validate an ^{18}F labeled small molecule VCAM-1 affinity ligand and demonstrate the feasibility of imaging VCAM-1 expression by PET-CT in murine arteries.

Background—Hybrid PET-CT imaging may allow simultaneous assessment of atherosclerotic lesion morphology (CT) and biology through the development of novel tracers (PET), thus facilitating early risk assessment in individual patients.

Methods—A cyclic, a linear, and an oligomer affinity peptide, internalized into endothelial cells by VCAM-1–mediated binding, were initially derivatized with DOTA to determine their binding profiles and pharmacokinetics. The lead compound was then ^{18}F labeled and tested in apoE$^{-/-}$ mice as well as models of MI and heart transplant rejection.

Results—The tetrameric peptide had the highest affinity and specificity for VCAM-1 (97% inhibition with soluble VCAM-1). In vivo PET-CT imaging using ^{18}F-4V showed 0.31±0.02 SUV in murine atheroma (ex vivo %IDGT 5.9±1.5). ^{18}F-4V uptake colocalized with atherosclerotic plaques on Oil Red O staining, and correlated to mRNA levels of VCAM-1 measured by quantitative RT-PCR (R=0.79, p=0.03). Mice treated with atorvastatin had significantly lower lesional uptake ($p<0.05$). Furthermore, ^{18}F-4V imaging in myocardial ischemia and in transplanted hearts showed good correlation with ex vivo measurement of VCAM-1 mRNA.

Conclusion—^{18}F-4V allows noninvasive PET-CT imaging of VCAM-1 in inflammatory atherosclerosis, has the dynamic range to quantify treatment effects and correlates with inflammatory gene expression.

Corresponding author: Ralph Weissleder, MD, PhD, MGH-CSB, CPZN-5206, 185 Cambridge Street, Boston, MA 02124, Tel: 617-726-8226, Fax: 617-726-5708, rweissleder@mgh.harvard.edu.
*These authors contributed equally

Conflict of Interest Disclosures: None.

Keywords

atherosclerosis; molecular imaging; inflammation; VCAM-1; PET-CT

Introduction

A reliable non-invasive diagnostic strategy for detecting inflamed arterial lesions at risk for complications could help target and evaluate therapies to prevent myocardial infarction and stroke. Current clinical imaging technologies largely provide structural information (1); however, the anatomical severity of stenosis does not sufficiently gauge risk of vascular events (2). Molecular imaging approaches now in development aim to interrogate biological processes rather than morphology (1,3,4).

VCAM-1 plays a cardinal role in atherosclerotic plaque progression (5–7). Activated endothelial cells that line the tissue-blood interface express VCAM-1, as can lesional macrophages and smooth muscle cells (5–7). VCAM-1 mediates inflammatory cell adhesion through interaction with the integrin very late antigen-4 (8). The early induction, confinement of expression to atherosclerotic lesions, and accessible position in proximity to the blood pool render VCAM-1 an attractive imaging biomarker.

We (9,10) and others (11,12) have imaged VCAM-1 as a proof-of-principle in inflammatory disease, for instance with targeted nanoparticles for MRI. While providing early efficacy data, these agents face practical regulatory hurdles that prevent rapid clinical development. Despite the specific advantages of PET, the increasing clinical availability of PET-CT scanners, and the unmet need for noninvasive identification of high-risk vascular lesions, relatively few targeted PET agents exist for plaque imaging (13,14). ^{18}FDG can accumulate in atherosclerotic lesions (15–17) and is clinically approved for cancer imaging. Fluorodeoxyglucose uptake presumably indicates glucose transport, and uptake associates with macrophage (18) and neovessel content (19). Studies in patients undergoing endarterectomy (17) showed increased ^{18}FDG signal in macrophage-rich carotid arteries. However, there remains a need for development of agents that selectively target inflammation in plaques, and that have lower background uptake in metabolically highly active myocardial tissue than ^{18}FDG to facilitate coronary imaging.

Here we describe the design, synthesis, evaluation, and use of a new PET imaging agent with optimized pharmacokinetics and specificity for VCAM-1. The overall design of this peptide-based agent hinged on: a) preference of PET-CT as a hybrid clinical imaging modality with high sensitivity (PET) combined with detailed anatomical information (CT), b) choice of ^{18}F as a clinical PET tracer with a short half-life, c) harnessing powerful signal amplification strategies (multivalency of affinity ligand and VCAM-1–mediated cell internalization), and d) choice of a probe design that would ultimately allow for rapid clinical translation.

Materials and Methods

Agent synthesis

A number of VCAM-1 specific peptide sequences have been identified by phage display technology (9,10) containing linear and cyclic heptapeptides (Table 1, http://pepbank.mgh.harvard.edu/). To facilitate comparative testing of agents in the current work, we first derivatized 3 lead peptides with the chelator DOTA and labeled them with ^{111}Indium. Peptides were synthesized using standard FMOC chemistry, followed by HPLC analysis which demonstrated >98% purity. The labeling yields of ^{111}In-DOTA derivatives were >99% at specific activities of 30.8 GBq.μmol^{-1}. Based on initial comparative

results, we then redesigned the best peptide (sequence VHPKQHR, linker GGSYKKK, tetramer) and labeled it with ^{18}Fluorine using a benzaldehyde method (20). The synthesis of the lead compound, named ^{18}F-4V, was automated using a PETsynthRN synthesizer (Nebeling GmbH) followed by HPLC purification. We also synthesized a fluorescent version of ^{18}F-4V by conjugating Cy5 maleimide to enable fluorescence microscopy detection of the probe in histological sections.

Competition Assays

We evaluated the affinity of peptides in competition assays using murine VCAM-1 immobilized on agarose beads. TLP-DOTA-^{111}In (37GBq per μmole, 0.5nM) was added to VCAM-1/agarose beads, and competed off with increasing concentrations of unlabeled MCP-DOTA, MLP-DOTA, and TLP-DOTA, respectively. After washing, the amount of labeled TLP-DOTA-^{111}In bound to beads was quantitated via gamma well counter. Next we assessed binding of candidate peptides to VCAM-1 expressing endothelial cells. ^{111}In-labeled peptides were added to MHEC (21) and incubated at 37°C for 1 hour. Cells were harvested from the plates and the radioactivity measured via gamma well counter. To evaluate specificity for VCAM-1, ^{18}F-4V (0.20μg) was pre-incubated with 5x murine VCAM-1 or saline and then added to MHEC.

Mouse models

ApoE$^{-/-}$ mice had an average age of 45 weeks and were on a high-cholesterol diet (Harlan Teklad), which produces reliable VCAM-1 expression in atherosclerotic plaques located in the aortic root (10). To test imaging in the setting of therapy, we treated a cohort of apoE$^{-/-}$ mice with atorvastatin (enriched in diet, 0.01% wt/wt) (10). Two additional disease entities known to increase VCAM-1 expression were imaged: MI was induced by coronary ligation (22), and heterotopic allograft heart transplantation from BALB/C into C57/B6 mice was performed (23). Mice were anesthetized for all procedures (isoflurane 2–3% v/v, Baxter). The institutional subcommittee on research animal care approved all animal studies.

Biodistribution studies

The blood half-life of candidate probes was determined with serial retro-orbital bleeds after injection of 150 μCi of a given agent into the tail vein of 6 wild-type mice. After sacrifice (4hrs), mice were perfused with 10ml of saline. Organs were harvested and their activity was recorded with a gamma counter (1480 Wizard 3″, PerkinElmer). Biodistribution data was corrected for decay and residual activity at the injection site. Oil Red O staining depicted the distribution of plaques in apoE$^{-/-}$ aortas, which were consequently analyzed by digital autoradiography. To evaluate the in vivo specificity of ^{18}F-4V, cohorts of mice were pre-injected with an antibody targeted to VCAM-1 (BD Pharmingen), followed by ^{18}F-4V 60 minutes later.

Fluorescence and immuno-histology

One hour after injection of Cy5 labeled 125**μ**g peptide, aortas were harvested for fluorescence microscopy and immunohistochemical detection of VCAM-1 (CD106), endothelial cells (CD31), macrophages (MAC-3, all BD Pharmingen) and smooth muscle cells (**α**-actin, Lab Vision).

PET-CT imaging

PET imaging was initiated 1 hour after injection of ^{18}F-4V (325±167μCi in 200±65μL) in conjunction with high-resolution vascular CT (Inveon, Siemens). PET data was reconstructed with OSEM and FBP algorithms (24), with a spatial resolution approaching ~1mm. For quantitation of PET signal, region of interests were placed in the aortic root based on anatomical

CT imaging. The CT x-ray source was used with a power of 80 kVp and 500 μA, an exposure time of 370–400 ms and an isotropic resolution of 90 μm. During CT acquisition, Isovue-370 (Bracco Diagnostics) was infused intravenously.

Quantitative RT-PCR

To validate in vivo PET data, we correlated ^{18}F-4V uptake to expression of VCAM-1 and CD68 quantified by multiplex quantitative PCR (TaqMan, Applied Biosystems) with GAPDH as an endogenous control.

Statistics

Results are expressed as mean±SEM. Unpaired data were compared using the unpaired two-sided t test, and for paired data using the paired two-sided t-test. The significance level in all tests was 0.05. Due to space limitations of the format, the method section has been abbreviated.

RESULTS

In vitro and in vivo screening of candidate peptides

To determine the affinity of candidate compound, we measured displacement of radioactively tagged TLP bound to purified VCAM-1 by cold MLP, MCP, or TLP. Sigmoidal concentration-dependence curves were observed with R^2 of 0.984 (TLP), 0.9880 (MLP), and 0.9934 (MCP) (Fig. 1A). The tetrameric, linear peptide formulation TLP had an IC_{50} for VCAM-1of 86.6 nM, 232- and 349-fold better than MCP or MLP, respectively.

We then screened candidates against MHEC, which constitutively express high levels of VCAM-1 (21), and observed significantly higher accumulation of TLP than that of MLP or MCP (Fig 1B). Finally, candidate peptides injected into apoE$^{-/-}$ mice facilitated evaluation of uptake into atheroma. TLP showed the highest %IDGT in excised aortas 60 minutes after injection (4.8-fold higher than MLP and 2.4-fold higher than MCP), corroborated by highest signal on autoradiography exposure (Fig. 1C and D).

Specificity, biodistribution, and half-life of ^{18}F-4V

We next proceeded to synthesize the PET tracer ^{18}F-4V by labeling the lead peptide TLP with ^{18}F via ^{18}fluorobenzaldehyde (Fig. 2). Cell uptake experiments involving inhibition with soluble VCAM-1 resulted in a 97% activity decrease, demonstrating specificity of ^{18}F-4V (Fig. 3A).

We injected ^{18}F-4V injected into 6 wild-type mice to established the blood half-life and biodistribution. ^{18}F-4V had a blood half-life of 16±0.6min (R^2 of fit = 0.96). The biodistribution at 4 hours transpired as follows (%IDGT): kidney, 13.2±2.8; liver, 3.7±1.1; lymph node, 3.7 ±0.3; spleen, 2.1±0.6; lung, 2.2±0.8; small intestine 1.9±0.4; fat, 1.7±0.1; skin, 1.7±0.6; stomach, 1.7±1.1; esophagus, 1.5±0.5; blood, 1.5±0.4; large intestine, 1.4±0.5; aorta, 1.3±0.4; bone, 1.3±0.4; thymus 0.9±0.3; skeletal muscle, 0.7±0.3; heart, 0.6±0.2; and feces, 0.2±0.1.

^{18}F-4V accumulates in atherosclerotic plaques

We assessed uptake of ^{18}F-4V into atherosclerotic plaques in excised aortas of wild-type mice, apoE$^{-/-}$ mice, and apoE$^{-/-}$ mice treated with atorvastatin. When compared to wild type, uptake in the aortic root was 312% higher in apoE$^{-/-}$ mice ($p < 0.05$, Fig. 3B). Autoradiography and en face Oil Red O staining confirmed that activity concentrated in atherosclerotic plaques (Fig. 3C). Treatment with atorvastatin significantly reduced uptake of ^{18}F-4V (Fig. 3B).

To assess the selectivity of in vivo uptake of ^{18}F-4V for VCAM-1, we pre-injected apoE$^{-/-}$ mice with 250 μg of monoclonal VCAM-1–antibody. This procedure reduced the uptake of the agent to levels seen in wild-type mice (Fig. 3B).

The cellular and microscopic distribution of the agent was assessed using a fluorescently labeled version of the tetrameric peptide and showed good correlation with immunoreactive VCAM-1 expression (Fig. 4). The probe distributed mainly to endothelial and subendothelial layers, and colocalized primarily with endothelial cells.

In vivo PET-CT imaging of ^{18}F-4V detects VCAM-1 expression in atherosclerotic plaques

Dynamic PET imaging identified 60–120 min after injection as the optimal time period for acquisition (Fig. 5). At that time, we found strong focal PET signal in the aortic root of apoE$^{-/-}$ mice (Fig. 6). Hybrid imaging facilitated unambiguous allocation of PET signal to the vascular bed of interest identified by contrast-enhanced vascular CT. Absolute quantification of PET signal (standard uptake value, SUV) showed significantly higher values in the root of apoE$^{-/-}$ compared to atorvastatin-treated apoE$^{-/-}$ or wild-type mice (Fig. 6).

Uptake of ^{18}F-4V closely correlates with inflammatory gene expression

After imaging, we determined the ex vivo activity of aortic sections and assessed gene expression by RT-PCR (Fig. 7). ^{18}F-4V-derived activity correlated with VCAM-1 mRNA levels ($R=0.79$, $p=0.03$, Fig. 7). We also explored gene expression of CD68, a macrophage biomarker of inflammatory atherosclerosis ($R^2 = 0.50$, $p<0.05$).

VCAM-1 imaging in other cardiovascular disorders

Given the above results, we reasoned that ^{18}F-4V PET imaging could apply to variety of other cardiovascular conditions, e.g., ischemic myocardial injury or transplant rejection, situations which may involve widespread VCAM-1–mediated monocyte recruitment. We assayed VCAM-1 transcript levels in mice 5 days after MI and on day 7 after heart transplantation. VCAM-1 mRNA levels increased 20-fold and 3-fold, respectively. As in atherosclerosis, inflamed myocardium had considerable uptake of ^{18}F-4V (Fig. 8). The specificity of this uptake was investigated in vivo with blocking of uptake by pre-injection with a VCAM-1 targeted antibody, which reduced the infarct activity to background ratio from 3.1 to 1.4, and in the transplant model the graft to background ratio from 2.4 to 1.4.

DISCUSSION

The central role of VCAM-1 in the evolution of inflammatory vascular lesions and its exposed, accessible position on the endothelial surface render this adhesion molecule an attractive imaging target for atherosclerosis, MI and transplant rejection. Here we show that PET-CT can image VCAM-1 and describe the design, synthesis, and validation of the novel PET imaging agent ^{18}F-4V. The technique detects VCAM-1 expression in murine aortas, vessels with a diameter considerably smaller than epicardial human coronary arteries. We also show that targeting VCAM-1 is useful for imaging of other cardiovascular diseases.

The initial design of three candidate probes derived from peptides identified by phage display (9,10). Although all of these peptides did target VCAM-1, the modified imaging probes differed in their affinity, molecular weight, and pharmacokinetics. TLP, the lead peptide with the highest affinity and most favorable pharmacokinetics, had an arborizing, tetrameric design. The multivalency of TLP resulted in superior performance, a phenomenon previously observed for targeted nanoparticles (25). Consequently, we derivatized TLP with the clinical PET tracer ^{18}F and investigated ^{18}F-4V in a number of in vitro and in vivo experiments. In vitro, pre-incubation of the agent with soluble VCAM-1 almost completely blocked cellular uptake.

In vivo, pre-injection of a VCAM-1–specific antibody blocked ^{18}F-4V uptake, and ^{18}F-4V signal correlated closely to VCAM-1 mRNA levels in respective vascular territories (R=0.79). Areas of highest activity colocalized with Oil Red O–stained atherosclerotic plaques on excised aortas. Statin treatment, known to reduce VCAM-1 expression (26), diminished ex vivo and in vivo ^{18}F-4V signal. The biodistribution of ^{18}F-4V proved favorable, with low background uptake in undiseased vessel walls and a short blood half-life, which will allow for rapid injection-imaging sequences.

VCAM-1 expression contributes to the pathophysiology of a variety of other cardiovascular conditions, for instance to inflammation after ischemic injury (11,22,27). MI triggers a profound influx of neutrophils and monocytes on days 1–6 after ischemia, and the quantity as well as quality of the myeloid cell influx determine the degree of ensuing heart failure and therefore prognosis (27–29). As an integral part of the recruiting mechanism for monocytes, VCAM-1 expression could gauge the degree of inflammation after MI. We found a substantial increase of VCAM-1 mRNA levels in mice on day 5 after coronary ligation, consistent with ^{18}F-4V accumulation. VCAM-1 also rises during cardiac transplant rejection, and promotes monocyte recruitment into the graft (30,31). Mononuclear phagocytes constitute up to 60% of the inflammatory cell population during parenchymal rejection (32). Patients after heart transplantation would greatly benefit from noninvasive assessment of rejection, since repetitive endomyocardial biopsies, the current reference standard, involve invasion and carry a risk of complication. VCAM-1 mRNA levels increased in heterotopically transplanted cardiac allografts, and ^{18}F-4V signal indeed rose in these rejecting allografts.

Compared to previous efforts to visualize VCAM-1 by MRI or ultrasound (9,10,12,33), ^{18}F-4V imaging provides a number of potential advantages. PET affords absolute signal quantification and will allow robust and noninvasive measurement of VCAM-1 expression, critical for assessment of individual patients as well as patient cohorts in clinical trials. Not only do high affinity and specificity for a target essential to lesion biology support the translatability of ^{18}F-4V, so too do its employment of a clinically established PET tracer and its clinically useful probe design. The inherent sensitivity of PET allows detection of targets at concentrations that are several orders of magnitude lower than seen with other modalities, for instance MRI. This feature may have particular importance when targets are as small as atherosclerotic plaques.

Acknowledgments

The authors acknowledge the help of Peter Waterman, BS, Gregory Wojtkiewicz, MS, Brett Martinelli, BS, Yoshiko Iwamoto, BS, and Timur Shtatland, PhD.

Funding sources: This work was funded in part by the D.W. Reynolds Foundation (PL, RW), UO1-HL080731 (RW), R01-HL078641 (RW), and R24-CA92782 (RW).

Abbreviations

VCAM-1	Vascular Cell Adhesion Molecule-1
^{18}F-4V	^{18}F labeled tetrameric peptide, PET imaging reporter targeted to VCAM-1
^{18}FDG	[^{18}F]-fluorodeoxyglucose
MCP	Monomeric Cyclic Peptide (DOTA labeled)
MLP	Monomeric Linear Peptide (DOTA labeled)
TLP	Tetrameric Linear Peptide (DOTA labeled)

DOTA	1,4,7,10-tetraazadodecane-1,4,7,10-tetraacetic acid, chelator for 111-Indium labeling
MHEC	murine heart endothelial cells
MI	Myocardial Infarction
%IDGT	percent injected dose per gram tissue

References

1. Sanz J, Fayad ZA. Imaging of atherosclerotic cardiovascular disease. Nature 2008;451(7181):953–957. [PubMed: 18288186]
2. Falk E, Shah PK, Fuster V. Coronary plaque disruption. Circulation 1995;92(3):657–671. [PubMed: 7634481]
3. Cyrus T, Lanza GM, Wickline SA. Molecular imaging by cardiovascular MR. J Cardiovasc Magn Reson 2007;9(6):827–843. [PubMed: 18066742]
4. Jaffer FA, Libby P, Weissleder R. Molecular imaging of cardiovascular disease. Circulation 2007;116(9):1052–1061. [PubMed: 17724271]
5. Iiyama K, Hajra L, Iiyama M, Li H, DiChiara M, Medoff BD, Cybulsky MI. Patterns of vascular cell adhesion molecule-1 and intercellular adhesion molecule-1 expression in rabbit and mouse atherosclerotic lesions and at sites predisposed to lesion formation. Circ Res 1999;85(2):199–207. [PubMed: 10417402]
6. Li H, Cybulsky MI, Gimbrone MA Jr, Libby P. Inducible expression of vascular cell adhesion molecule-1 by vascular smooth muscle cells in vitro and within rabbit atheroma. Am J Pathol 1993;143(6):1551–1559. [PubMed: 7504883]
7. Libby P, Li H. Vascular cell adhesion molecule-1 and smooth muscle cell activation during atherogenesis. The Journal of Clinical Investigation 1993;92(2):538–539. [PubMed: 7688759]
8. Libby P. Inflammation in atherosclerosis. Nature 2002;420(6917):868–874. [PubMed: 12490960]
9. Kelly KA, Allport JR, Tsourkas A, Shinde-Patil VR, Josephson L, Weissleder R. Detection of vascular adhesion molecule-1 expression using a novel multimodal nanoparticle. Circ Res 2005;96(3):327–336. [PubMed: 15653572]
10. Nahrendorf M, Jaffer FA, Kelly KA, Sosnovik DE, Aikawa E, Libby P, Weissleder R. Noninvasive vascular cell adhesion molecule-1 imaging identifies inflammatory activation of cells in atherosclerosis. Circulation 2006;114(14):1504–1511. [PubMed: 17000904]
11. Behm CZ, Kaufmann BA, Carr C, Lankford M, Sanders JM, Rose CE, Kaul S, Lindner JR. Molecular imaging of endothelial vascular cell adhesion molecule-1 expression and inflammatory cell recruitment during vasculogenesis and ischemia-mediated arteriogenesis. Circulation 2008;117(22):2902–2911. [PubMed: 18506006]
12. McAteer MA, Sibson NR, von Zur Muhlen C, Schneider JE, Lowe AS, Warrick N, Channon KM, Anthony DC, Choudhury RP. In vivo magnetic resonance imaging of acute brain inflammation using microparticles of iron oxide. Nature Medicine 2007;13(10):1253–1258.
13. Elmaleh DR, Fischman AJ, Tawakol A, Zhu A, Shoup TM, Hoffmann U, Brownell AL, Zamecnik PC. Detection of inflamed atherosclerotic lesions with diadenosine-5′,5‴-P1,P4-tetraphosphate (Ap4A) and positron-emission tomography. Proceedings of the National Academy of Sciences of the United States of America 2006;103(43):15992–15996. [PubMed: 17038498]
14. Nahrendorf M, Zhang H, Hembrador S, Panizzi P, Sosnovik DE, Aikawa E, Libby P, Swirski FK, Weissleder R. Nanoparticle PET-CT imaging of macrophages in inflammatory atherosclerosis. Circulation 2008;117(3):379–387. [PubMed: 18158358]
15. Rudd JH, Myers KS, Bansilal S, Machac J, Pinto CA, Tong C, Rafique A, Hargeaves R, Farkouh M, Fuster V, Fayad ZA. Atherosclerosis Inflammation Imaging with 18F-FDG PET: Carotid, Iliac, and Femoral Uptake Reproducibility, Quantification Methods, and Recommendations. J Nucl Med 2008;49(6):871–878. [PubMed: 18483100]
16. Rudd JH, Warburton EA, Fryer TD, Jones HA, Clark JC, Antoun N, Johnstrom P, Davenport AP, Kirkpatrick PJ, Arch BN, Pickard JD, Weissberg PL. Imaging atherosclerotic plaque inflammation

with [18F]-fluorodeoxyglucose positron emission tomography. Circulation 2002;105(23):2708–2711. [PubMed: 12057982]

17. Tawakol A, Migrino RQ, Bashian GG, Bedri S, Vermylen D, Cury RC, Yates D, LaMuraglia GM, Furie K, Houser S, Gewirtz H, Muller JE, Brady TJ, Fischman AJ. In vivo 18F-fluorodeoxyglucose positron emission tomography imaging provides a noninvasive measure of carotid plaque inflammation in patients. Journal of the American College of Cardiology 2006;48(9):1818–1824. [PubMed: 17084256]
18. Aziz K, Berger K, Claycombe K, Huang R, Patel R, Abela GS. Noninvasive detection and localization of vulnerable plaque and arterial thrombosis with computed tomography angiography/positron emission tomography. Circulation 2008;117(16):2061–2070. [PubMed: 18391115]
19. Calcagno C, Cornily JC, Hyafil F, Rudd JH, Briley-Saebo KC, Mani V, Goldschlager G, Machac J, Fuster V, Fayad ZA. Detection of neovessels in atherosclerotic plaques of rabbits using dynamic contrast enhanced MRI and 18F-FDG PET. Arterioscler Thromb Vasc Biol 2008;28(7):1311–1317. [PubMed: 18467641]
20. Poethko T, Schottelius M, Thumshirn G, Hersel U, Herz M, Henriksen G, Kessler H, Schwaiger M, Wester HJ. Two-step methodology for high-yield routine radiohalogenation of peptides: (18)F-labeled RGD and octreotide analogs. J Nucl Med 2004;45(5):892–902. [PubMed: 15136641]
21. Allport JR, Lim YC, Shipley JM, Senior RM, Shapiro SD, Matsuyoshi N, Vestweber D, Luscinskas FW. Neutrophils from MMP-9- or neutrophil elastase-deficient mice show no defect in transendothelial migration under flow in vitro. Journal of Leukocyte Biology 2002;71(5):821–828. [PubMed: 11994507]
22. Nahrendorf M, Sosnovik D, Chen JW, Panizzi P, Figueiredo JL, Aikawa E, Libby P, Swirski FK, Weissleder R. Activatable magnetic resonance imaging agent reports myeloperoxidase activity in healing infarcts and noninvasively detects the antiinflammatory effects of atorvastatin on ischemia-reperfusion injury. Circulation 2008;117(9):1153–1160. [PubMed: 18268141]
23. Shimizu K, Libby P, Shubiki R, Sakuma M, Wang Y, Asano K, Mitchell RN, Simon DI. Leukocyte integrin Mac-1 promotes acute cardiac allograft rejection. Circulation 2008;117(15):1997–2008. [PubMed: 18378617]
24. Hudson HM, Larkin RS. Accelerated image reconstruction using ordered subsets of projection data. IEEE transactions on medical imaging 1994;13(4):601–609. [PubMed: 18218538]
25. Weissleder R, Kelly K, Sun EY, Shtatland T, Josephson L. Cell-specific targeting of nanoparticles by multivalent attachment of small molecules. Nat Biotechnol 2005;23(11):1418–1423. [PubMed: 16244656]
26. Aikawa M, Sugiyama S, Hill CC, Voglic SJ, Rabkin E, Fukumoto Y, Schoen FJ, Witztum JL, Libby P. Lipid lowering reduces oxidative stress and endothelial cell activation in rabbit atheroma. Circulation 2002;106(11):1390–1396. [PubMed: 12221058]
27. Nahrendorf M, Swirski FK, Aikawa E, Stangenberg L, Wurdinger T, Figueiredo JL, Libby P, Weissleder R, Pittet MJ. The healing myocardium sequentially mobilizes two monocyte subsets with divergent and complementary functions. The Journal of Experimental Medicine 2007;204(12):3037–3047. [PubMed: 18025128]
28. Maekawa Y, Anzai T, Yoshikawa T, Asakura Y, Takahashi T, Ishikawa S, Mitamura H, Ogawa S. Prognostic significance of peripheral monocytosis after reperfused acute myocardial infarction:a possible role for left ventricular remodeling. Journal of the American College of Cardiology 2002;39(2):241–246. [PubMed: 11788214]
29. Mariani M, Fetiveau R, Rossetti E, Poli A, Poletti F, Vandoni P, D'Urbano M, Cafiero F, Mariani G, Klersy C, De Servi S. Significance of total and differential leucocyte count in patients with acute myocardial infarction treated with primary coronary angioplasty. European Heart Journal 2006;27(21):2511–2515. [PubMed: 16923741]
30. Herskowitz A, Mayne AE, Willoughby SB, Kanter K, Ansari AA. Patterns of myocardial cell adhesion molecule expression in human endomyocardial biopsies after cardiac transplantation. Induced ICAM-1 and VCAM-1 related to implantation and rejection. Am J Pathol 1994;145(5):1082–1094. [PubMed: 7977640]
31. Tanaka H, Sukhova GK, Swanson SJ, Cybulsky MI, Schoen FJ, Libby P. Endothelial and smooth muscle cells express leukocyte adhesion molecules heterogeneously during acute rejection of rabbit cardiac allografts. Am J Pathol 1994;144(5):938–951. [PubMed: 7513950]

32. Hancock WW, Thomson NM, Atkins RC. Composition of interstitial cellular infiltrate identified by monoclonal antibodies in renal biopsies of rejecting human renal allografts. Transplantation 1983;35 (5):458–463. [PubMed: 6342225]

33. Kaufmann BA, Sanders JM, Davis C, Xie A, Aldred P, Sarembock IJ, Lindner JR. Molecular imaging of inflammation in atherosclerosis with targeted ultrasound detection of vascular cell adhesion molecule-1. Circulation 2007;116(3):276–284. [PubMed: 17592078]

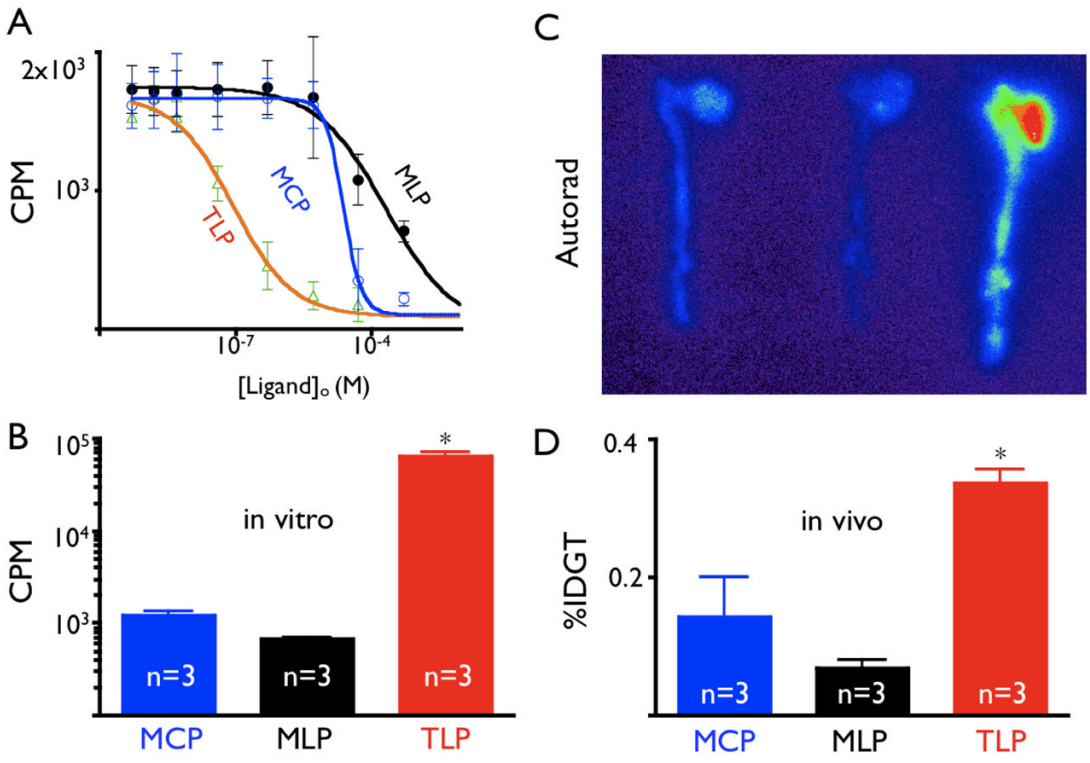

Figure 1.

1A: Affinity curves for candidate ligands assessed by competition after binding to immobilized VCAM-1. CPM: Counts per minute. Mean ± 95% confidence interval.

1B: Cell uptake assay after incubation of MHEC with peptides.

1C: ApoE$^{-/-}$ mice of equivalent age were injected with ^{111}In labeled peptides.

1D: %IDGT in aortas excised from apoE$^{-/-}$ after injection of TLP, MCP, and MLP, *p<0.05.

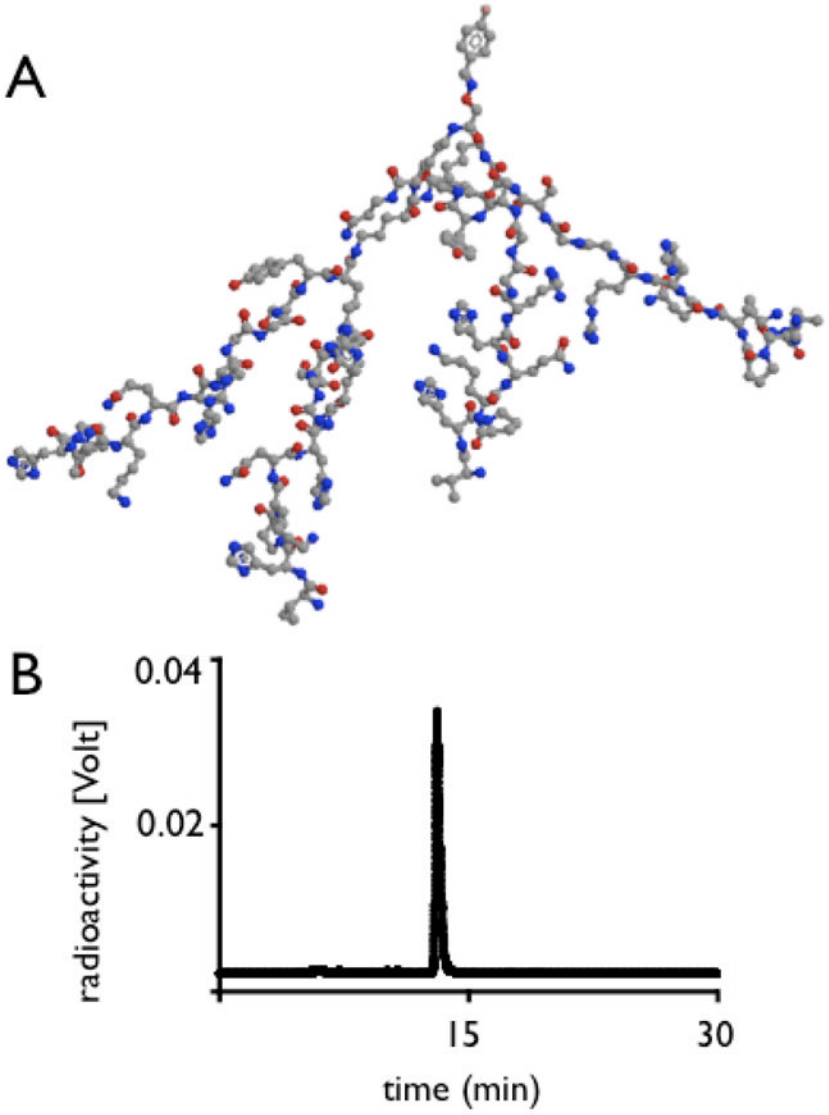

Figure 2.
2A: Three-dimensional model of ^{18}F-4V. The tracer ^{18}F is located on the top, and the 4 branching affinity peptides point downward.
2B: Original HPLC trace of ^{18}F-4V.

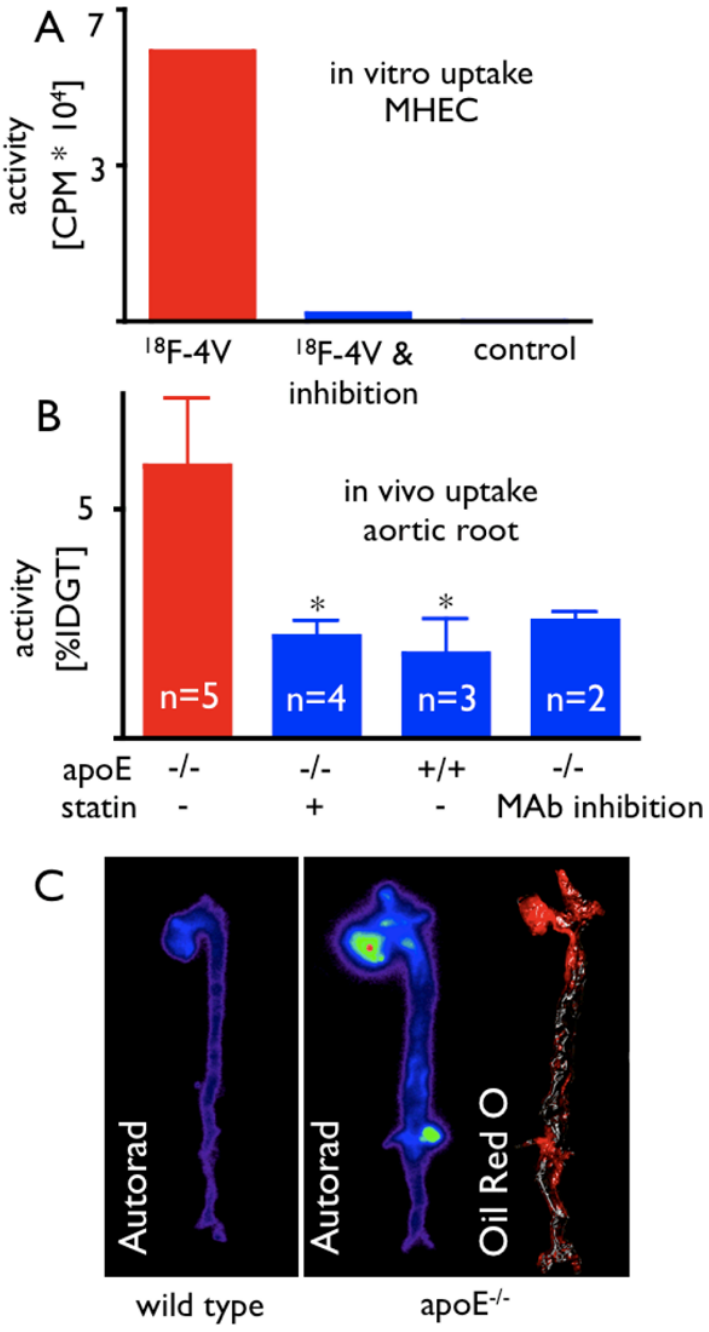

Figure 3.

3A: Pre-incubation of the probe with soluble VCAM-1 significantly reduces uptake of ^{18}F-4V into MHEC. CPM: Counts per minute.

3B: Uptake of ^{18}F-4V in excised aortas by scintillation counting. MAb: preinjection of a monoclonal VCAM-1–targeted antibody, *$p<0.05$.

3C: Exposure of aortas on a phosphorimager corroborates highest uptake of ^{18}F-4V in apoE-deficient mice, with little uptake in wild-type aortas. Oil Red O staining shows peak uptake in plaques.

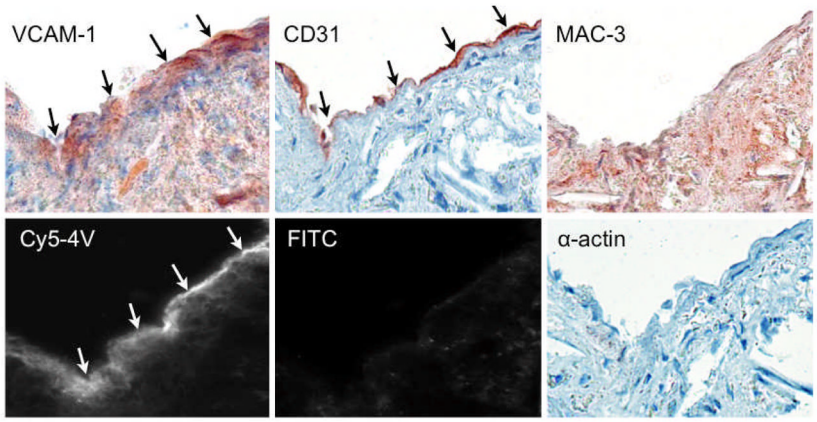

Figure 4.

A fluorescent version of ^{18}F-4V (cy5-4V) was used to explore histological distribution. The endothelial and subendothelial layers of an atherosclerotic plaque show strong uptake, while autofluorescence in the FITC channel is neglible. On adjacent sections, VCAM-1 and endothelial staining colocalize with the agent, with some uptake in macrophages and smooth muscle cells. Magnification 400×.

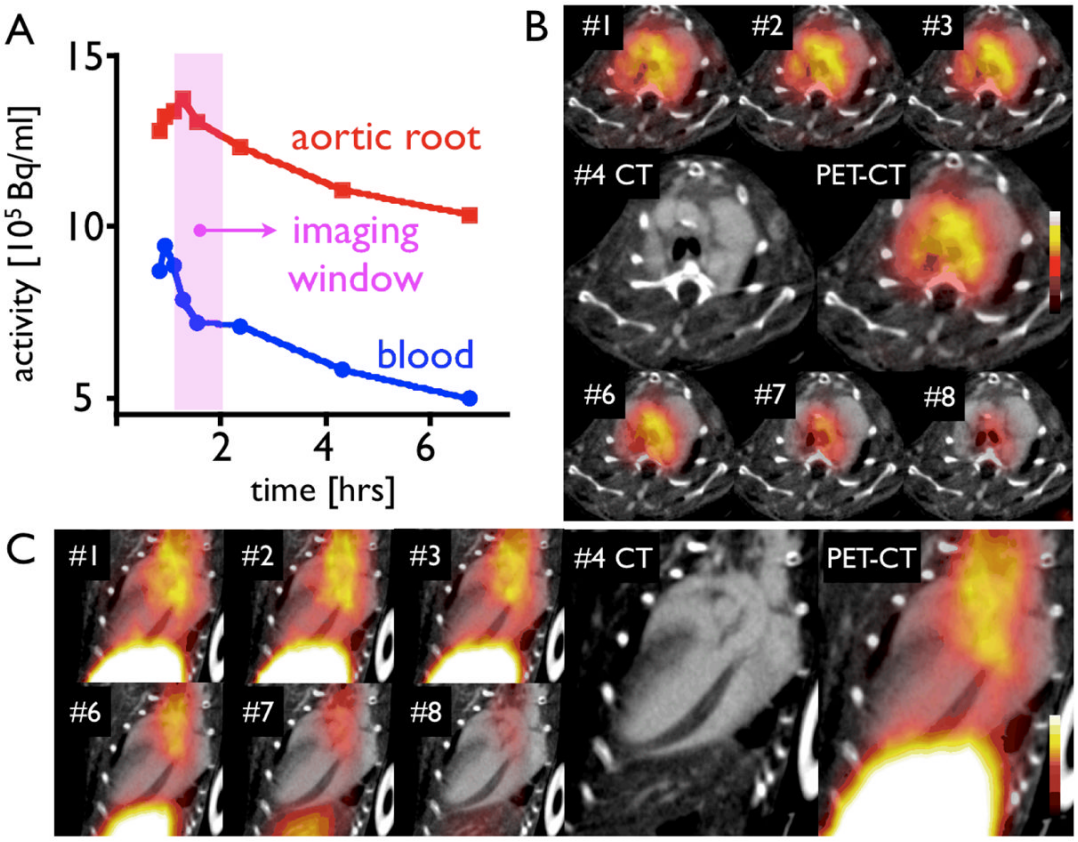

Figure 5.
Dynamic PET imaging identified 60–120 minutes after injection as a suitable time window. Blood activity was measured in the left ventricular blood pool. Signal in the blood pool and the aortic root is plotted (A) and shown over time in short (B) and long axis (C) PET-CT.

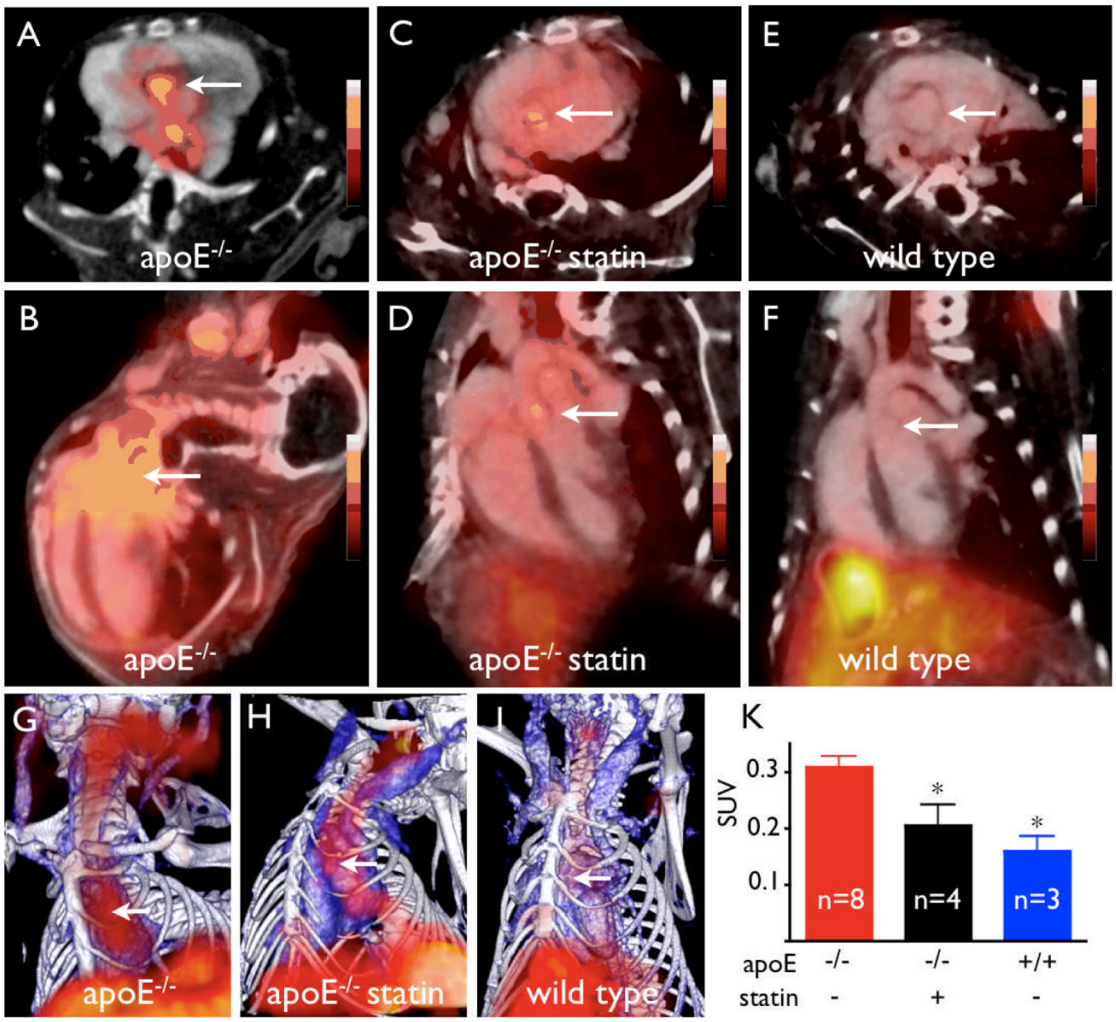

Figure 6. PET-CT imaging in apoE$^{-/-}$ and statin treated mice

A, C, E: short-axis PET-CT images of the aortic root (arrows).

B, D, F: long-axis views.

G, H, I: 3D maximum intensity projection (bone=white, vasculature+blue, ^{18}F-4V=red).

K: PET signal as SUV (standard uptake value), *p<0.05.

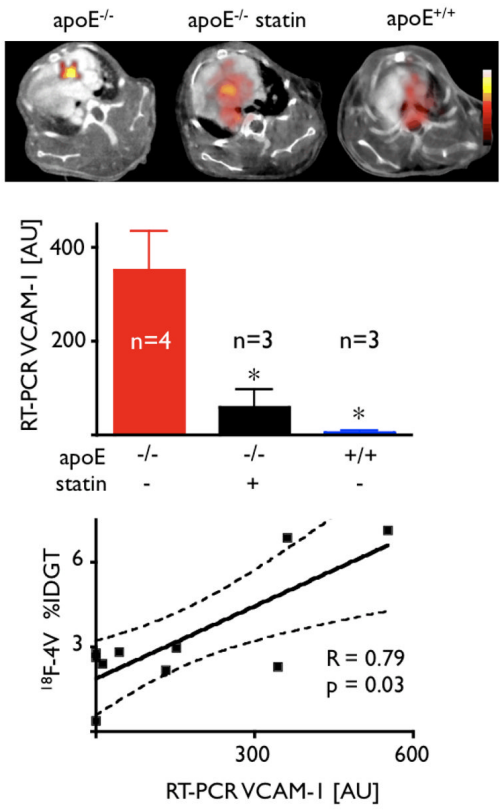

Figure 7.
Correlation of ^{18}F-4V uptake to VCAM-1 expression by quantitative RT PCR, *p<0.05.

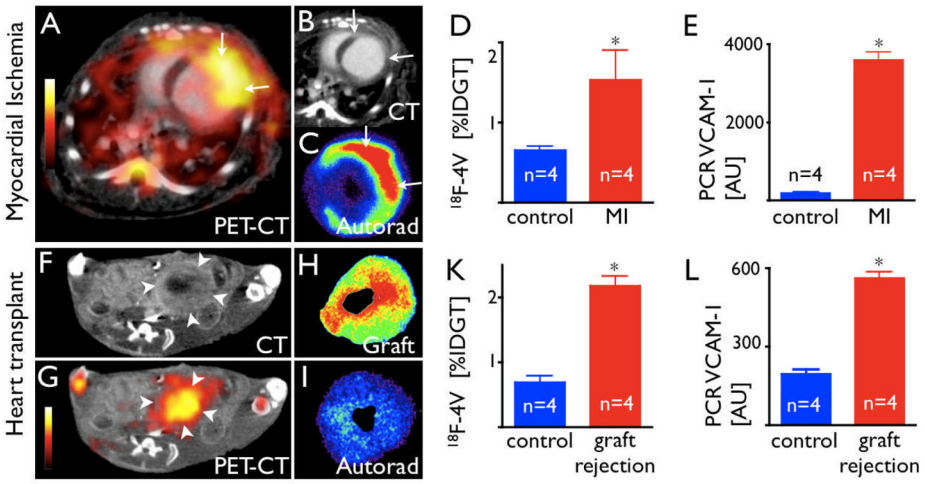

Figure 8.

8A: PET-CT 5 days after MI shows strong signal in the infarcted LV wall.

8B: Contrast-enhanced CT depicts MI (arrows).

8C: Autoradiography of myocardial ring.

8D: %IDGT in the infarct and in non-infarcted myocardium.

8E: VCAM-1 mRNA, AU: Arbitrary units.

8F, G: PET-CT of a mouse heart transplanted heterotopically into the abdominal cavity. The rejected allograft (arrow heads) shows high uptake of ^{18}F-4V.

8H, I: Autoradiography of the graft and the orthotopic recipient heart.

8K: Uptake of ^{18}F-4V in rejected allografts.

8L: VCAM-1 mRNA levels on day 7 after transplantation, *p<0.05.

Table 1

Summary of specific VCAM-1 targeted peptide sequences

Name	Peptide Sequence	Linear/Cyclic	Monomer/Tetramer
MCP	CVHSPNKKCGGSYSK(DOTA)	Cyclic	Monomer
MLP	VHPKQHRGGSYK(DOTA)	Linear	Monomer
TLP	$((VHPKQHRGGSY)_2)K)_2KK$(DOTA)	Linear	Tetramer
^{18}F-4V	$((VHPKQHRGGSY)_2)K)_2KK$(AOE)	Linear	Tetramer